

Anisotropic, Strong, and Thermally Insulating 3D-Printed Nanocellulose–PNIPAAm Aerogels

Yannick Nagel, Deeptanshu Sivaraman, Antonia Neels, Tanja Zimmermann, Shanyu Zhao, Gilberto Siqueira,* and Gustav Nyström*

Cellulose is a promising candidate for the fabrication of superinsulating materials, which would be of great interest for thermal management applications as well as for the scientific community. Until now, the production of strong cellulose-based aerogels has been dominated by traditional manufacturing processes, which have limited the possibilities to achieve the structural control and mechanical properties seen in natural materials such as wood. In this work, we show a simple but versatile method to fabricate cellulose aerogels in intricate geometries. We take advantage of the 3D printing technique direct ink writing to control both the shape and the thermal-mechanical properties of the printed cellulose-based hydrogel inks. Moreover, the shear forces involved in the extrusion process allow us to impart an anisotropic nanostructure to the printed samples. By solvent exchange and supercritical drying, the hydrogel parts are then transformed into stable aerogels. Using X-ray diffraction analysis, mechanical tests and thermal conductivity tests, our 3D printed aerogels are shown to exhibit directionally dependent thermal-mechanical properties higher than those reported for earlier cellulose-based aerogels. These characteristics enable us to fabricate customized structures that can be precisely tailored for their application as load-bearing insulating materials for thermal management.

notable development in the use of renewable energy sources in the past decades, conventional energy resources such as oil or coal are still dominating the energy market.^[2] To limit the damage on the environment, it is of paramount importance to develop new technologies that not only reduce the use of fossil fuels, but also drastically improve the efficiency of the generated and consumed energy. The construction industry stands out for the substantial amount of energy spent throughout the life cycle of a building, given by the energy used for heating (31%) and for cooling (12%).^[3] To reduce the energy consumption, it is essential to find ways to use environmentally friendly materials that are effective in thermal management. Insulation materials from natural sources have been widely commercialized and their price-to-performance ratio makes them favorable candidates to solve this issue.^[4] However, some of them require energy-intensive processing technologies (glass wool, stone wool, polystyrene) and


1. Introduction

The planetary demand for energy is steadily increasing,^[1] fueled by the constantly rising global population, by the push for urbanization and industrial globalization. While there has been a

complex waste management, while bio-based fiber materials have a slightly lower performance (kenaf, wood fiber) than synthetic materials.^[5] Among all thermal insulation materials, aerogels have outstanding physical properties and hold record-breaking low thermal conductivity.^[6] Silica aerogels show

Y. Nagel, T. Zimmermann, G. Siqueira, G. Nyström
Cellulose & Wood Materials Laboratory
Empa – Swiss Federal Laboratories for Materials Science and Technology
8600 Dübendorf, Switzerland
E-mail: gilberto.siqueira@empa.ch; gustav.nystroem@empa.ch

D. Sivaraman, S. Zhao
Laboratory for Building Energy Materials and Components
Swiss Federal Laboratories for Materials Science and Technology
Empa
8600 Dübendorf, Switzerland

 The ORCID identification number(s) for the author(s) of this article can be found under <https://doi.org/10.1002/sstr.202300073>.

© 2023 The Authors. Small Structures published by Wiley-VCH GmbH. This is an open access article under the terms of the Creative Commons Attribution License, which permits use, distribution and reproduction in any medium, provided the original work is properly cited.

DOI: 10.1002/sstr.202300073

A. Neels
Center for X-Ray Analytics
Swiss Federal Laboratories for Materials Science and Technology
Empa
8600 Dübendorf, Switzerland

G. Siqueira
Complex Materials
Department of Materials
ETH Zürich
8093 Zürich, Switzerland

G. Nyström
Department of Health Science and Technology
ETH Zürich
8092 Zürich, Switzerland

thermal superinsulation, that is, λ less than $20 \text{ mW m}^{-1} \text{ K}^{-1}$, and are currently the best industry-ready performing material.^[7] However, due to their fragile and dusty nature, there is strong interest in the community in finding a suitable ecological alternative material. One promising alternative is represented by aerogels produced starting from naturally occurring macromolecules. In fact, it has already been demonstrated that aerogels could be produced starting from gelatin, agar, chitosan, and cellulose.^[8] In particular, cellulose in an aerogel form is a promising candidate to form superinsulating materials,^[9,10] as it combines an inherently low thermal conductivity with its intrinsically renewable aspects.^[11] Besides, cellulose is a very flexible material which can be processed down to its nanocomponents to generate building blocks for the production of more complex materials.^[12,13] Indeed, cellulose nanofibrils (CNFs) and cellulose nanocrystals (CNCs) can help attain materials which are structured over different length scales and are inspired by the design principles of nature. Nature provides us with multiple examples of how simple building blocks, when organized in an efficient manner at the nano- and at the microscale, can give rise to properties that exceed those of the starting materials. The most prominent examples of such natural architectures are wood, mammalian cortical bone, and nacre.^[14,15] In all of these materials, the common natural design principle lies in the specific organization of long and stiff nano- and microfibrils or of high-aspect-ratio particles to achieve local control of the mechanical and thermal properties. In the field of nanocellulose-based materials, this has been achieved using different fabrication strategies. Using a "top-down" approach, it is possible to produce cellulose scaffolds with exceptional mechanical and thermal properties starting from the delignification of a bulk piece of wood.^[16,17] This process allows retention of the beneficial hierarchical wood structure and cellulose directionality within the scaffolds. Conversely, it is also possible to apply a "bottom-up" assembly by initially extracting the nanocellulose building blocks and using them as reinforcing elements in composites prepared by additive processes like 3D printing. This method allows the preparation of composites with a high degree of particle/fiber alignment^[9,18–20] and freedom to customize the parts. Alternatively, also self-assembled nanocellulose structures with chiral nematic order have been exploited to make strong aerogels^[21] but compared to the previous methods, this route is more time-consuming and the freedom of shape of the final materials is limited.

Despite the great improvements in mechanical and thermal properties that were accomplished in previous studies,^[9,16,21] the intricate structures and the extraordinary local control of properties seen in biological materials have not yet been fully matched. The ability to replicate such multidimensional control would allow us to produce materials with better overall properties as well as to design parts that are tailored to meet specific demands.

In the field of thermal management, fabrication of materials that are able to influence heat flow in an efficient manner, while ensuring sufficient mechanical stability for the applied load case, is of great interest. Addressing such thermal mechanical challenges using naturally sourced materials represents an economical and environmentally friendly approach to obtain

more sustainable insulation while minimizing the use of energy-intensive resources.

In this work, biosourced aerogels with exceptional anisotropic thermal-mechanical properties are produced by controlling the arrangement of nanocellulose particles in a gel structure. To illustrate the advantages of microstructural manipulation, we used a "bottom-up" approach to manufacture CNC-based aerogels via 3D printing, that have stiffness of up to 65 MPa in one direction, while exhibiting outstanding insulating properties ($32 \text{ mW m}^{-1} \text{ K}^{-1}$) in the other. The nanocellulose alignment in different directions was verified by 2D wide-angle scattering (2D WAXS) analysis on supercritical dried samples, supporting our claims of structure and alignment-induced property control. Similar methods for 3D printing CNC-based aerogels have already been illustrated^[22–25] in the past. This particular approach offers a simple and unique way to produce application-specific aerogels that match loading and thermal insulation criteria. The focus of the work is on a method for better structural control to improve the mechanical and thermal performance of CNC-based aerogels. Although the CNC-based aerogels are not limited in mechanical and thermal performance properties, this method could be applied to improve and tailor these properties as well as be transferred to other fields.^[25] Different than other particle orientation methods, like ice templating,^[23] this method offers complete freedom to arrange the reinforcing building blocks in space. In addition, it also illustrates how additive manufacturing can be used to control porosity of aerogels^[22] to modulate their thermal property and possibly other properties. We envision these materials to have a great impact in various sectors, especially where controlled porosity and mechanical stability play an important role, such as in the electronics and in the textile industries but also in the tissue engineering and drug delivery fields.

2. Results & Discussion

2.1. Manufacturing of Complex-Shaped Aerogels

The manufacturing of complex-shaped aerogel composites was achieved through four main steps: first by formulation of cellulose-based hydrogel inks; second by 3D printing highly ordered microstructures; third by crosslinking of a polymer network by UV light; and finally by supercritical carbon dioxide drying (scCO_2). The production schematic of these functional cellulose-based aerogels is further illustrated in **Figure 1**.

A characteristic step of this process is the forced alignment of the nanocrystals inside the ink filaments, which determines the final mechanical and thermal properties of the aerogel. Additive manufacturing (AM) allows for spatial arrangements of these properties, tuning them efficiently to match a required shape and application. As previously shown,^[26–28] the main prerequisite for successful 3D printing, and more in detail direct ink writing (DIW) of soft materials, is the formulation of a highly homogeneous ink with shear-thinning behavior (**Figure 1a**). The rheological behavior of the formulated ink is important as we do not induce any phase change (like in Fused Deposition Modelling (FDM) printing) and the ink should be solid enough to withstand the tendency to flow and to hold its own weight.

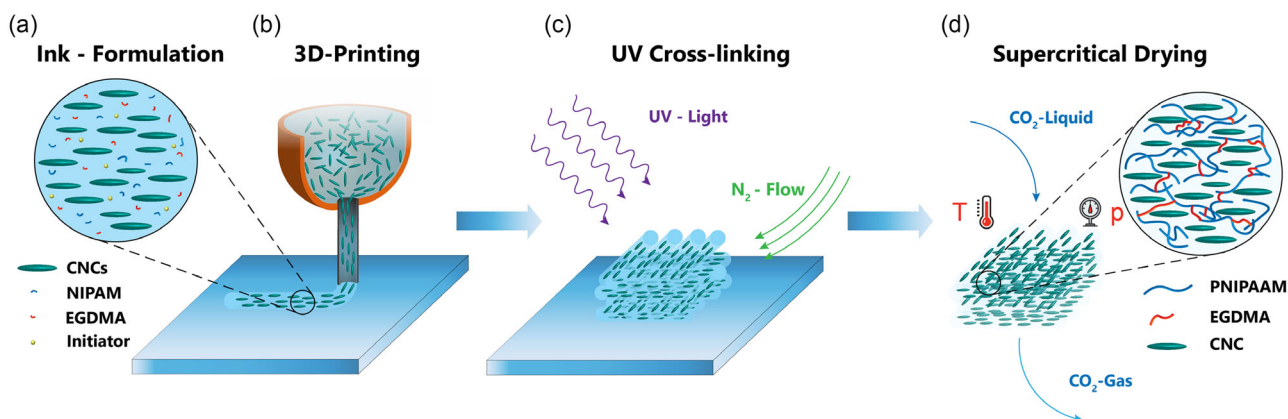


Figure 1. Schematic of the steps involved in the 3D printing of functional cellulose-based aerogels. a) Ink formulation and production. b) DIW of cellulose-based hydrogels. c) Post-treatment to cure the printed structure into functional parts. d) Supercritical drying of ethanol solvent-exchanged cellulosic gels to obtain aerogels.

The ink system considered in this work consists of a certain amount of monomer, photoinitiator, and crosslinking agent which are dispersed together with CNCs in water (Figure S1, Supporting Information). The CNCs tend to form a percolating network that can be extruded through a syringe and yields self-standing structures, which was verified by rheological studies. Furthermore, due to their aspect ratio ($AR = 18$) and mechanical strength, the CNC particles can act as both the rheological modifier of the ink and as mechanical reinforcement for the resulting composite material.^[29] Increasing the amount of CNC particles will increase the stiffness of the final material, while also changing its processing conditions. It is therefore important to find the ideal formulation that optimizes all these parameters to achieve desired material properties. Nonetheless, the ink formulation is very simple and flexible when compared to other 3D-printed technologies like stereolithography (SLA) printing.

2.2. Gel Formulation and Rheological Properties

For the process of AM through the DIW method, inks that present viscoelastic behavior are required. This can be achieved by tuning the rheology of highly concentrated CNC dispersions to allow for ideal 3D printing performance and for the alignment of the anisotropic nanoparticles.^[30] Shear and extensional forces generated by the extrusion process have been proven to be the reason for the orientation of anisotropic particles like CNCs^[30] and this alignment in turn influences the final mechanical and thermal properties of our system. In addition, a sufficiently high yield stress and elastic modulus are necessary to produce dimensionally stable parts.^[26] To validate these characteristics, rheological characterization has been performed. The results of the continuous and oscillatory rotation tests for inks containing 10, 15, and 20 wt% of CNCs are shown in Figure 2a,b. The resulting yield stresses and moduli are crucial for the choice of the formulation more suitable for 3D printing. Based on previous research on nanocellulose inks for 3D printing,^[19] we found solid content of 20 wt% CNC, with a true yield stress of 249 Pa and a storage modulus of 5.3 MPa, to be the best for our process. Using

a simplified model^[30] (Supporting Information), it is possible to give an estimated printing pressure range needed for successful alignment of the particles. Depending on the composition of the ink and the choice of nozzle for the extrusion process, the ideal range of pressure for particle orientation will change.

In this work, we take advantage of the full control on the rheological properties of nanocellulose-based systems and the affinity of nanocellulose with water to prepare high-nanocellulose-loaded monomer/polymer-based hydrogels for DIW. In order to retain the shape of the printed object and to further increase the mechanical properties and the layer adhesion, strengthening or gelation of the network is required.^[31] For this purpose, we used poly(*N*-isopropylacrylamide) (PNIPAAm) in combination with the crosslinking additive ethyldimethacrylate (EGDMA) as a multifunctional polymer system^[32,33] (Figure 2c). During ink production and storage, adequate UV protection equipment were used, so that prepolymerization did not occur prior to printing. Polymerization and crosslinking was then induced by the radicals generated by a photoinitiator, which upon UV light illumination yields a strong hydrogel after printing.^[32] The aerogels composite samples are then prepared by subjecting the additively manufactured hydrogels to a stepwise solvent exchange from water to ethanol that can be accelerated by increased temperatures. The steady increase in the ethanol content helps to prevent swelling of the matrix because of Ostwald ripening.^[34] Using this method, the printed parts can be processed for supercritical drying with minimal distortion. Small objects, like 5 mm × 5 mm × 5 mm cubes, can be produced from ink preparation to final aerogel in less than 24 h.

2.3. Aerogel Composites Mechanical Properties

To get the anisotropic properties of our composites, we tune the manufacturing parameters to achieve the highest possible alignment of the nanocellulose building blocks. As investigated in previous work^[26–28] on composites and hydrogels, the orientation of anisotropic particles during the extrusion process (Figure 3a) depends on two main criteria: the rheology of the ink (Figure 2a) and the flow conditions during processing.

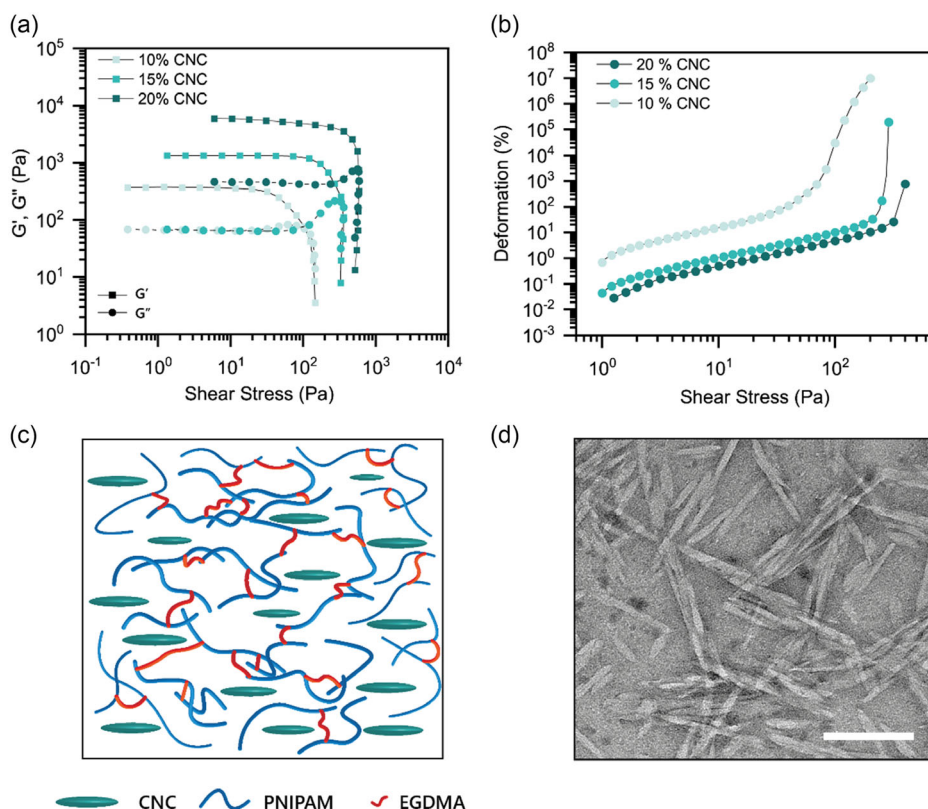


Figure 2. Rheological behavior of aqueous CNC inks, formulated by varying solid loading. a) Oscillatory rheological measurements (frequency (1 Hz)) of increasing CNC content (10, 15, and 20 wt% CNC). b) Yield stress measurements of increasing CNC loading. c) Schematic illustration of CNC PNIPAM hydrogels. d) Transmission electron microscopy (TEM) image of cellulose nanocrystals (Scale bar: 100 nm).

Our motivation to preserve the 3D-printed network of cellulose-loaded inks was facilitated by gentle supercritical drying of the ordered structures. To verify if the printing conditions were optimized and if alignment was preserved in the final aerogels, we quantified the alignment of nanocellulose in 3D-printed unidirectional films, single filaments, and in the intersection between filaments in grid-like structures using 2D WAXS (Figure 3b,c). In addition, SEM images were taken on fractured printed filaments (Figure S2, Supporting Information) to visually access the alignment of CNCs in the printed structures.

Unidirectional aerogel films were made by printing discontinuous lines close to each other, the width of the filaments corresponds to the smallest diameter of the conical nozzle used (0.41 mm). The diameter of the nozzle also determines the current resolution of the printed parts. To ensure adhesion between the filaments and the substrate, the distance between the lines was chosen to be slightly smaller than their diameter (0.40 mm), as well as the layer height was set to 80% of it (0.32 mm). This way the extruded filaments are compressed onto the previous layer (or the substrate), ensuring a higher contact surface between the filaments. Under these conditions, we see no particular alignment or orientation for the baseline NIPAAm matrix in comparison to the aerogel with CNC (Figure 3b). The CNC containing aerogel on the other hand shows a clear 2D WAXS pattern, with two clear intensity peaks with an 180° phase difference, indicating good alignment induced by the cellulose nanoparticles. To compare these

materials to our previous studies^[19] and to further investigate the influence of the printing conditions, the same measurements were performed on single filaments and intersection points between filaments (grid-like structures). The resulting two-intensity peaks of a single filament are even sharper than the ones of the film and give the highest degree of orientation 0.72 (calculated as explained in Supporting Information and presented in Table S1, Supporting Information). This value is comparable to previous publications,^[19,22,27,32] which show around 0.65–0.70° of alignment (π). Compared to previous studies, here the measures are taken on supercritical dried aerogels. At the point of intersection between two filaments, we still measure very strong alignment. However, it is clear that the contact between filaments perturbs the CNC alignment.

These results indicating well-aligned CNC particles within the printed materials are supported by the SEM images (Figure S2b, Supporting Information) and therefore translated into aerogels with exceptionally high anisotropic mechanical properties (Figure 3d,e). To characterize the mechanical performance of our anisotropic CNC-based aerogels, compression tests were performed on samples with different raster directions (Figure S3, Supporting Information). Samples printed unidirectionally (0° filling) were loaded parallel (longitudinal) and transversely (transverse) to the printing direction. Stress–strain data (Figure 3d) show remarkable differences between the two loading conditions. In the transverse direction, the samples show a typical cellulose aerogel response.^[35] It is characterized by an

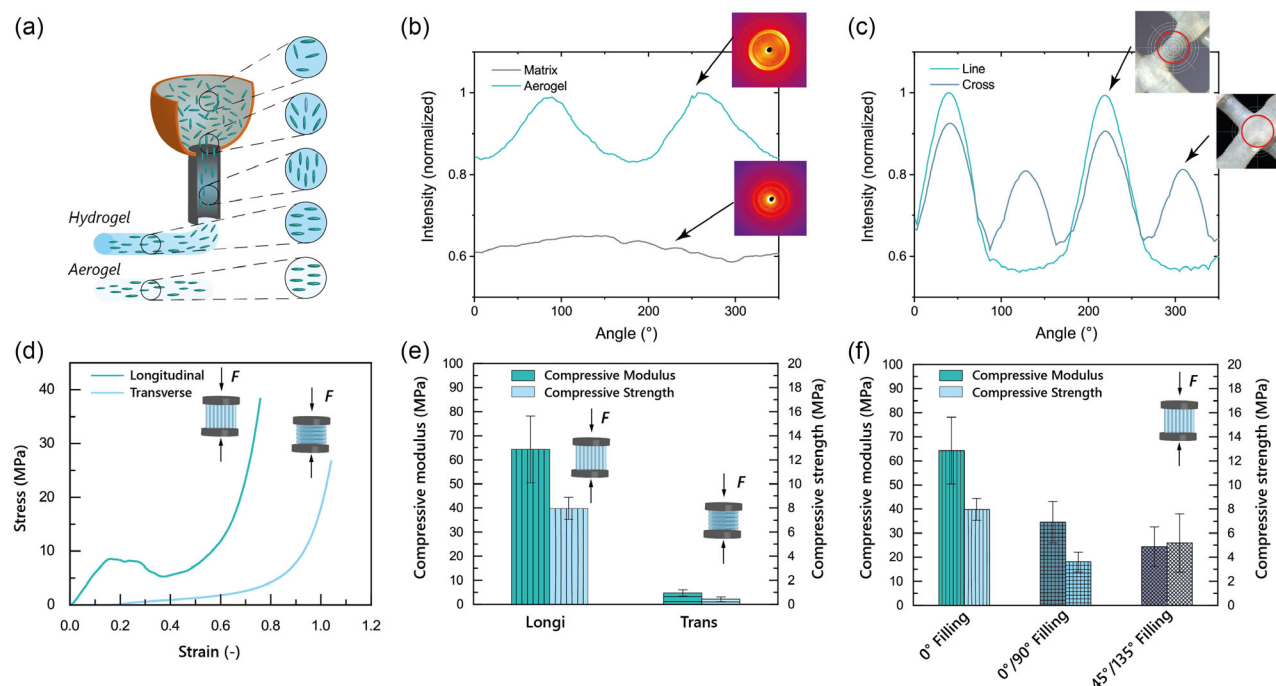


Figure 3. Enhanced mechanical properties of CNC–NIPAAm aerogels, containing 20 wt% of CNCs, tested in compression mode at longitudinal (Longi) and transverse (Trans) directions with different filling patterns. a) Schematic illustration of nanoparticle alignment in printing nozzle. b) Radially integrated intensity as a function of azimuthal angle of a unidirectional printed aerogel and the NIPAAm matrix (the insets show the 2D WAXS images) as well as c) single-aerogel filament and crossing point between perpendicular filaments (the insets show the probed sample volume on optical images). d) Typical stress–strain curves of samples tested in longitudinal and transverse direction. e) Compressive modulus and strength of CNC–NIPAAm aerogels with 0° filling tested in longitudinal and transverse direction. f) Compressive modulus and strength of CNC–NIPAAm aerogels with different infill directions (0°, 0°/90°, and 45°/135°).

initial linear viscoelastic behavior,^[36] followed by a constant stress plateau indicative of gradual pore collapse with further alignment perpendicular to the compression direction and a final disintegration and densification of the porous structure.^[37] Longitudinally tested structures show a different response, more characteristic for polymer composites (Figure S4, Supporting Information). In the beginning, they exhibit a linear response up to 15% of strain, followed by a region of plastic buckling of the porous particle structure; after that, the typical breakage of the porous network and densification of the matrix can be seen.^[11] The different shape of the stress–strain curves is a clear indication for the anisotropy of the material. The samples with nanocellulose aligned parallel to the applied stress reach a compression modulus of 64 ± 14 MPa, which is one order of magnitude higher than the ones tested transverse to the print direction (Table S2, Supporting Information). This anisotropy is also notable in the compression strength, with the samples tested in the longitudinal direction, showing compression strength of 8.0 ± 0.9 MPa, which is 20 times higher than the ones tested in the transverse direction. Nonunidirectional printed samples, including raster angles of 0°/90° and 45°/135° were tested under compression (Figure 3f). Both patterns have much lower compressive properties than the 0° fill samples in the longitudinal testing configuration. This confirms that the increase in stiffness of the composites is directly proportional to the volume fraction of particles aligned in the measurement direction. On the other hand, when testing the samples perpendicular to the printing

direction, the 0°/90° infill raster shows the better mechanical performance, while the unidirectional samples have the worst performance (Table S2, Supporting Information). High compression modulus and strength, in combination with AM, make it possible to fabricate complex bioinspired parts with mechanical properties tuned for the required load cases. Nonetheless, our CNC-based formulation shows very brittle behavior. This could be improved by locally tuning the composition of the material as for example by the addition of CNF or by modifying the cellulose–polymer interface.

2.4. Anisotropic Thermal Insulation of 3D Printed Aerogels

In this work we show how to fabricate complex cellulose-based aerogels which exhibit a unique combination of mechanical strength and low thermal conductivity. Compared to traditional manufacturing methods like casting or molding, our method has several advantages: there is no need for any templates or molds' prefabrication. In addition, it is possible to improve and control the properties of the aerogel. Furthermore, due to the layer-by-layer fabrication and achieved cellulose alignment, these aerogel structures are interesting for functional confinement of particles and molecules. Possible examples are the thermoelectric effect, where oriented cellulose structures lead to selective diffusion of ions, increasing the effect by orders of magnitudes,^[38,39] catalytic and chemoselective effects, where the confinement of nanoparticles can lead to increased efficiencies,^[40] and the

thermal conductivity, where the confinement of air particles leads to anisotropic thermal properties.^[17] In fact, here we display anisotropic thermal properties (Figure 4a,b), which make these aerogels an interesting candidate for thermal management applications.

Thermal measurements were performed perpendicular to the print plane (transverse) and parallel along the print direction (longitudinal). The transverse tested samples show low thermal conductivity $\lambda = 32.8 \text{ mW m}^{-1} \text{K}^{-1}$, whereas longitudinally tested samples have almost twofold increased values ($\lambda = 56.1 \text{ mW m}^{-1} \text{K}^{-1}$). The high degree of alignment owing to both 3D printing and scCO_2 drying assures that we achieve these unique properties, in comparison to freeze drying and mold casting of the same samples.^[41] The thermal properties of the nanocellulose aerogels are dominated by their mesoporous structure and the Knudsen effect for such pores, which was confirmed by the characteristic Brunauer–Emmett–Teller (BET) curves (Figure S2, Supporting Information) and an average pore size of $40 \pm 2 \text{ nm}$ ^[42] resulting in low λ values.^[35] The higher thermal conductivity measured along the printing direction can be explained by a hierarchical effect. Microscopically, DIW process unavoidably creates defects, spaces between the printed lines. This defects add up and lead to elongated pores throughout the printed structures, air channels similar to the lumen in mature wood. Swelling and shrinkage effects occur during solvent exchange and drying, additionally influencing the distorted pore network along the print direction, but ultimately enabling thermal conduction through the air channels.^[17,22] On the nano-scale, the alignment of anisotropic CNCs in the measurement

direction results in higher thermal conduction along this direction, in contrast to the reduction in average pore diameter in the perpendicular direction (transverse). The anisotropy is best visible when subjecting our material to small temperature gradients, for example, when worn on the human body and exposed to the surrounding ambient temperature (Figure 4a). As a demonstration, we printed two aerogels with different print directions, one with filaments transverse to a heat source and one with filaments longitudinal to the source. When placed on the arm of a person (35°C), thermal images reveal temperature variations that are directly linked to the anisotropy of the material. The temperature difference between the configurations is about 2°C . In Figure 4c, we see different structures printed with the transverse orientation, square, and hexagon vase geometries. These structures highlight the manufacturability of CNC-NIPAAm hydrogels (bottom structures) through 3D printing and the thermal insulation effect of the corresponding aerogels (top IR heat map). The thermal insulating properties of this type of aerogels can be locally manipulated by making use of the processing technology (3D printing), for example, by varying the density in the structure. In more detail, the cube in Figure 4c mimics the structure of double-pane windows by creating an air gap between two layers of aerogels. The air gap creates an additional insulating layer that slows down the transfer of heat through the structure; a schematic illustration can be found in the Figure S5, Supporting Information. Moreover, by combining aerogel and air insulation, it is possible to create a highly effective insulating system that provides both the excellent insulating properties of aerogel and the cost-effective simplicity of air insulation.

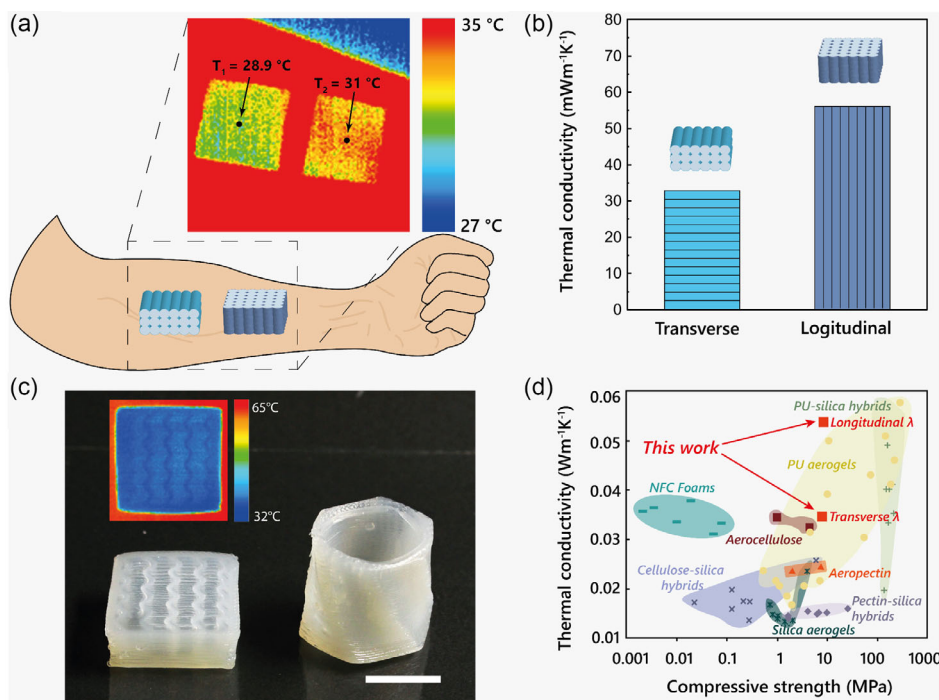


Figure 4. Complex cellulose-based aerogels with unique mechanical strength and thermal properties. a) Infrared image and schematics of cellulose aerogels placed on human arm. b) Thermal conductivity measurements of 3D-printed cellulose aerogels in transverse (perpendicular to print direction) and longitudinal (parallel to printing direction) direction. c) Photograph and infrared image of 3D-printed complex-shaped hydrogels scale bar is 10 mm d) Thermal conductivity versus final compressive strength for different aerogel-like materials. Adapted with permission.^[8] Copyright 2018, Wiley-VCH.

Figure 4d shows an Ashby plot of different aerogels with differing mechanical and thermal properties. Our samples show similar transverse thermal properties to other cellulose-based aerogels but mostly much higher mechanical stability. In longitudinal direction we can achieve higher thermal conductivity as the 3D-printing process orients the cellulose and creates air channels through the sample. We also show competitive aerogel hybrid thermal conductivities, which in combination with anisotropy, different thicknesses, and complex shapes offers new possibilities to manage heat for such 3D-printed aerogel networks. There are several ways to further improve the insulating properties of 3D-printed cellulose aerogels. We would like to mention two of them, the decrease of porosity via densification, which can be achieved through mechanical loading or wet densification,^[27] and the combination with other materials, for example, graphene oxide^[43] or silica.^[42]

3. Conclusion

In this work, we demonstrate a facile route for the fabrication of cellulose-based aerogels with tailorable mechanical and thermal properties. The use of CNCs allows us to fine tune the rheological properties of the starting hydrogels, making them suitable as inks for 3D printing by direct ink writing. The alignment of the cellulose achieved during printing is maintained by scCO₂ drying, resulting in aerogels with outstanding anisotropic properties. For instance, we show how a 0° longitudinal fill pattern possesses compression strength and elastic modulus about one order of magnitude higher than its transversal counterpart. Similarly, we record a twofold increase in thermal conductivity for the 0° longitudinal pattern when compared to the transversal one. Finally, our versatile method can be easily adapted to other polymeric matrices or even to prepare aerogels entirely composed of nanocellulose with very controlled particle orientations. This opens up the possibility to fabricate a wide range of bioinspired aerogels possessing multiple functionalities. We envision our approach to be of relevance in various fields including sustainable insulation, thermal management, thermoelectrics, and biomedicine.

4. Experimental Section

Materials: N-isopropylacrylamide (NIPAAm; 97%), photoinitiator Irgacure 2959 (98%), crosslinker ethylene glycol dimethacrylate (EGDMA; 98%), and glucose (99.5%) were purchased from Sigma-Aldrich (Buchs, Switzerland). Glucose oxidase (high purity), 2, 2,2,6,6-Tetramethyl-1-piperidinyloxy (TEMPO), was purchased from VWR International. CNCs from sulfuric acid hydrolysis of eucalyptus pulp produced at the USDA Forest Service –Forest Products Laboratory (Madison, WI) were purchased from University of Maine as freeze-dried powder.

Sample Preparation: For the production of 20 g of ink, 4 g of CNCs and 1.6 g of NIPAAm were mixed with 14.1 g of deionized water for 5 min at 1400, 2000, 2500, and 3500 rpm, respectively, in a speed mixer (model DAC 150.1 FVZ). The resulting gel contained 20 wt% CNC and 8 wt% NIPAAm. This cellulose-based gel was left for swelling for one night; after adding 1 g of EGDMA and 0.158 g of glucose, it was again mixed at 3500 rpm for 5 min. In a final step, 0.1 g of Irgacure 2959 and 0.0095 g of glucose oxidase were added and mixed at 1300 rpm for 5 min. The Irgacure 2959 photoinitiator was chosen based on its narrow absorption

range, water solubility, and widespread usage for biomedical applications. These properties provided a significant advantage by creating a longer processing time window during the DIW process. Before further processing and printing, the gel was filled in plastic cartridges and centrifuged for 5 min at 2000 rpm to remove air bubbles. The aqueous gels were then printed into scaffolds using a DIW from EnvisionTEC (Bioplotter Manufacturing series), which had a build volume of 150 × 150 × 150 mm and an axis resolution of 0.001 mm. The gels were extruded through conical plastic nozzles (0.41 mm in diameter) by applying between 1 and 2 bars of air pressure to 30 cc cartridges at 10 °C. After 3D printing, a 3D crosslinking of the CNC-based hydrogel was triggered by illuminating freshly printed parts with UV light under nitrogen atmosphere to reduce the inhibition of the monomer (NIPAAm). To prevent unwanted exposure to UV light prior to crosslinking, the majority of the printing operations were carried out in a dark environment, reducing the risk of premature polymerization and enabling better control over the printing process.

After the procedural solvent exchange, the gel was put in an autoclave and sealed in the supercritical drying system (Separex, France). The pressure of the system was gradually increased up to 120 bar for 1 h by introducing CO₂ with recirculation, while the temperature was set to 50 °C. The solvent was extracted through CO₂ circulation at 120 bar for 4 h. Then, the pressure was gradually decreased to ambient pressure over 1 h, to yield an aerogel sample.

Density: All analyzed samples were monolithic and regular in shape; therefore, envelope density could be directly evaluated using a balance and calipers. All density values are reported in the Table S2, Supporting Information.

BET Surface Area: A sample (particle size ≈ 3 mm) of measured mass (typically ≈ 100 mg) was placed in a special glass tube and vacuumed to a pressure of 0.016 mbar for 20 h at 100 °C (heating rate of 10 °C min^{−1}). The samples were weighed again and the nitrogen sorption isotherms analyzed from P/P₀ ranging from 0.001 to 0.998 in 40 steps, equilibration times of 10 s for each incremental nitrogen addition, and a minimum of 600 s per incremental step, leading to a total run time of 8–10 h. This analysis was repeated on three different 3D-printed aerogels.

2D WAXs: 2D wide-angle X-ray diffraction (2D WAXD, STOE IPS II, 0.71073 MoK α radiation source at 40 mA and 50 kV for 30 min, beam diameter of 0.5 mm in transmission mode) was used to study the degree of CNC alignment. The 3D-printed parts were fixed on the goniometer head and then placed perpendicular to the X-ray beam to allow the X-rays to pass through only the parts. The WAXD patterns were recorded on an Image Plate Detector System with a 340 mm diameter placed at a distance of 200 mm from the sample. For each on-sample position, a full image was recorded covering a 2 θ range from 3 to 40°. Azimuthal scans were integrated for the cellulose 200 reflection. The 2D WAXS spectra were recorded at multiple locations on one sample.

SEM: Scanning electron microscopy (SEM) images were obtained from a FEI Nova NanoSEM 230 instrument (FEI, Hillsboro, Oregon, USA) at an accelerating voltage of 5 kV and a working distance of 4 mm. The aerogels were coated with 10–15 nm of platinum before imaging at various magnifications.

Rheological Characterization: The rheological behavior of all the produced inks was characterized at 20 °C with an MCR 302 Anton-Paar rheometer in a plate–plate geometry with a 1 mm gap and a 50 mm plate diameter. In addition, a solvent trap was used to prevent evaporation. The ink was prepared, as described in the section Sample Preparation, but without the addition of 0.1 g of Irgacure 2959 and 0.0095 g of glucose oxidase to avoid uncontrolled polymerization that could damage the equipment as well as affect the measurement. Storage and loss moduli were measured with oscillatory strain variations from 0.01 to 1000% at a frequency of 1 Hz with logarithmic sweep. Apparent yield stress was defined as the shear stress when the storage and loss moduli intersected, that is, the gelation point. The rheological measurement was performed one time for each ink.

Mechanical Test: Compression tests were carried out on an AGS-X (Shimadzu) universal testing machine one 3D-printed cubes of the size

5 mm × 5 mm × 5 mm. At least three repeats for samples with different infill conditions were measured in transverse and longitudinal directions at a displacement rate of 1 mm min⁻¹. No preload was applied to the samples.

Thermal Conductivity Measurement: Thermal conductivity (λ) was measured with an in-house-guarded two-plate device,^[44] shielded to measure Z-axis uniaxial heat transfer coefficients. They were calibrated from industry standard measurements for a sample of 1000 mm × 1000 mm × 10 mm, according to ISO_12667/European Standard EN12667,^[42] to get relevant data for smaller samples. Produced samples were kept in a controlled atmosphere of 23 °C, 40% humidity for 24 h before measurements (for equilibrium with atmosphere). Temperature difference was kept at 10 °C with the cold plate at 20 °C and hot plate maintained at 30 °C. Each sample was measured for 1 h with calibrations for equilibration and steady-state heat flow present in the software. The measurement was performed on two samples of each configuration.

Supporting Information

Supporting Information is available from the Wiley Online Library or from the author.

Acknowledgements

The authors thank Anja Huch for help with transmission electron microscopy (TEM) of CNC solutions, Marco Binelli for the help with writing of the manuscript, and Carolina Reyes for help proofreading and language editing the manuscript.

Conflict of Interest

The authors declare no conflict of interest.

Data Availability Statement

The data that support the findings of this study are available from the corresponding author upon reasonable request.

Keywords

3D printing, aerogels, cellulose nanocrystals, hydrogels

Received: February 27, 2023

Revised: July 25, 2023

Published online: August 20, 2023

- [1] V. Apostolopoulou-Kalkavoura, P. Munier, L. Bergström, *Adv. Mater.* **2020**, *33*, 2001839.
- [2] S. Mathew, *Wind Energy*, Springer, Berlin **2006**.
- [3] S. Brida, in *United Nations Environmental Programme*, UN Publishing Service Section, Nairobi, Kenya **2009**.
- [4] F. Zou, T. Budtova, *Carbohydr. Polym.* **2021**, *266*, 118130.
- [5] F. Asdrubali, F. D'Alessandro, S. Schiavoni, *Sustainable Mater. Technol.* **2015**, *4*, 1.
- [6] N. Hüsing, U. Schubert, *Angew. Chem., Int. Ed.* **1998**, *37*, 22.
- [7] M. Koebel, A. Rigacci, P. Achard, *J. Sol-Gel Sci. Technol.* **2012**, *63*, 315.
- [8] S. Zhao, W. J. Malfait, N. Guerrero-Alburquerque, M. M. Koebel, G. Nyström, *Angew. Chem., Int. Ed.* **2018**, *57*, 7580.
- [9] Y. Kobayashi, T. Saito, A. Isogai, *Angew. Chem.* **2014**, *126*, 10562.
- [10] W. Chen, Q. Li, Y. Wang, X. Yi, J. Zeng, H. Yu, Y. Liu, J. Li, *ChemSusChem* **2014**, *7*, 154.
- [11] F. L. Dri, S. L. Shang, L. G. Hector, P. Saxe, Z. K. Liu, R. J. Moon, P. D. Zavattieri, *Modell. Simul. Mater. Sci. Eng.* **2014**, *22*, 085012.
- [12] G. Siqueira, J. Bras, A. Dufresne, *Polymers* **2010**, *2*, 728.
- [13] D. Zhao, Y. Zhu, W. Cheng, W. Chen, Y. Wu, H. Yu, *Adv. Mater.* **2021**, *33*, 2000619.
- [14] A. R. Studart, R. Libanori, R. M. Erb, *Bio- and Bioinspired Nanomaterials*, Wiley, Weinheim, Germany **2014**, pp. 335–368.
- [15] A. R. Studart, R. Libanori, R. M. Erb, *Materials Design Inspired by Nature: Function Through Inner Architecture*, The Royal Society of Chemistry, Cambridge, UK **2013**, pp. 322–358.
- [16] M. Frey, D. Widner, J. S. Segmehl, K. Casdorff, T. Keplinger, I. Burgert, *ACS Appl. Mater. Interfaces* **2018**, *10*, 5030.
- [17] T. Li, J. Song, X. Zhao, Z. Yang, G. Pastel, S. Xu, C. Jia, J. Dai, C. Dai, A. Gong, F. Jiang, Y. Yao, T. Fan, B. Yang, L. Wågberg, R. Yang, L. Hu, *Sci. Adv.* **2018**, *4*, eaar3724.
- [18] C. Thibaut, A. Denneulin, S. Rolland du Roscoat, D. Beneventi, L. Orgéas, D. Chaussy, *Carbohydr. Polym.* **2019**, *212*, 119.
- [19] G. Siqueira, D. Kokkinis, R. Libanori, M. K. Hausmann, A. S. Gladman, A. Neels, P. Tingaut, T. Zimmermann, J. A. Lewis, A. R. Studart, *Adv. Funct. Mater.* **2017**, *27*, 1604619.
- [20] J. Jiang, H. Oguzlu, F. Jiang, *Chem. Eng. J.* **2021**, *405*, 126668.
- [21] A. Tripathi, B. L. Tardy, S. A. Khan, F. Liebner, O. J. Rojas, *J. Mater. Chem. A* **2019**, *7*, 15309.
- [22] S. Sultan, A. P. Mathew, *Nanoscale* **2018**, *10*, 4421.
- [23] D. Kam, M. Chasnitsky, C. Nowogrodski, I. Braslavsky, T. Abitbol, S. Magdassi, O. Shoseyov, *Colloids Interfaces* **2019**, *3*, 46.
- [24] V. C. F. Li, C. K. Dunn, Z. Zhang, Y. Deng, H. J. Qi, *Sci. Rep.* **2017**, *7*, 8018.
- [25] A. J. Hess, A. J. Funk, Q. Liu, J. A. de La Cruz, G. H. Sheetah, B. Fleury, I. I. Smalyukh, *ACS Omega* **2019**, *4*, 20558.
- [26] B. G. Compton, J. A. Lewis, *Adv. Mater.* **2014**, *26*, 5930.
- [27] M. K. Hausmann, G. Siqueira, R. Libanori, D. Kokkinis, A. Neels, T. Zimmermann, A. R. Studart, *Adv. Funct. Mater.* **2019**, *1904127*, 1.
- [28] A. R. Studart, *Chem. Soc. Rev.* **2016**, *45*, 359.
- [29] A. Dufresne, *Cellulose and Potential Reinforcement*, De Gruyter, Berlin, Germany **2017**.
- [30] M. K. Hausmann, P. A. Rühs, G. Siqueira, J. Läger, R. Libanori, T. Zimmermann, A. R. Studart, *ACS Nano* **2018**, *12*, 6926.
- [31] J. Feng, B. L. Su, H. Xia, S. Zhao, C. Gao, L. Wang, O. Ogbeide, J. Feng, T. Hasan, *Chem. Soc. Rev.* **2021**, *50*, 3842.
- [32] O. Fourmann, M. K. Hausmann, A. Neels, M. Schubert, G. Nyström, T. Zimmermann, G. Siqueira, *Carbohydr. Polym.* **2021**, *259*, 117716.
- [33] X. Xu, Y. Liu, W. Fu, M. Yao, Z. Ding, J. Xuan, D. Li, S. Wang, Y. Xia, M. Cao, *Polymers* **2020**, *12*, 580.
- [34] S. Zhao, W. J. Malfait, E. Jeong, B. Fischer, Y. Zhang, H. Xu, E. Angelica, W. M. Risen, J. W. Suggs, M. M. Koebel, *ACS Sustainable Chem. Eng.* **2016**, *4*, 5674.
- [35] S. F. Plappert, J. M. Nedelec, H. Rennhofer, H. C. Lichtenegger, F. W. Liebner, *Chem. Mater.* **2017**, *29*, 6630.
- [36] L. Perin, A. Faivre, S. Calas-Etienne, T. Woignier, *J. Non-Cryst. Solids* **2004**, *333*, 68.
- [37] J. Gross, J. Fricke, *Nanostruct. Mater.* **1995**, *6*, 905.
- [38] D. Zhao, H. Wang, Z. U. Khan, J. C. Chen, R. Gabrielson, M. P. Jonsson, M. Berggren, X. Crispin, *Energy Environ. Sci.* **2016**, *9*, 1450.
- [39] T. Li, X. Zhang, S. D. Lacey, R. Mi, X. Zhao, F. Jiang, J. Song, Z. Liu, G. Chen, J. Dai, Y. Yao, S. Das, R. Yang, R. M. Briber, L. Hu, *Nat. Mater.* **2019**, *18*, 608.
- [40] J. Meng, Y. Liu, X. Shi, W. Chen, X. Zhang, H. Yu, *Sci. China Mater.* **2021**, *64*, 621.

- [41] L. Berglund, D. Sivaraman, S. Komulainen, V. Telkki, K. Oksman, *ACS Appl. Mater. Interfaces* **2021**, 13, 34899 .
- [42] S. Zhao, Z. Zhang, G. Sèbe, R. Wu, R. V. Rivera Virtudazo, P. Tingaut, M. M. Koebel, *Adv. Funct. Mater.* **2015**, 25, 2326.
- [43] B. Wicklein, A. Kocjan, G. Salazar-Alvarez, F. Carosio, G. Camino, M. Antonietti, L. Bergström, *Nat. Nanotechnol.* **2015**, 10, 277.
- [44] T. Stahl, S. Brunner, M. Zimmermann, K. Ghazi Wakili, *Energy Build.* **2012**, 44, 114.